JOURNAL OF COLLOID AND INTERFACE SCIENCE 171, 429–438 (1995)

The Influence of the Type of Flow on the Orthokinetic Coagulation Rate

L. L. M. KRUTZER, A. J. G. VAN DIEMEN, AND H. N. STEIN[1]

Laboratory of Colloid Chemistry, Department of Chemical Engineering, Eindhoven University of Technology, P.O. Box 513, 5600 MB, Eindhoven, The Netherlands

Received May 19, 1994; accepted October 12, 1994

The flow-induced behavior and Brownian coagulation behavior of a polystyrene latex were studied using a Coulter counter. The coagulation rates in Couette flow (either laminar or Taylor vortex flow), laminar pipe flow, and isotropic turbulent flow were compared with theoretical models. It was shown that the orthokinetic coagulation rate in laminar Couette flow, pipe flow, and isotropic turbulent flow can be described on the basis of existing theory but only when using a lower effective Hamaker constant than predicted from experiments on perikinetic coagulation. This means that the orthokinetic coagulation rate is lower than that predicted by theory. This agrees with measurements performed by other investigators. For Taylor vortex flow, however, the experimental dependence of the stability ratio on the parameter $N_{SA} = 6\pi\eta a^3\gamma/A$, where a is the particle radius, γ is the shear rate, and A is a Hamaker constant, is different from that predicted by theory. From experiment and theory it is clear that at equal energy dissipation the coagulation rate is highest for the isotropic turbulent flow.

INTRODUCTION

Orthokinetic coagulation processes have been studied rather intensively during the past decades, both theoretically (see e.g. (1–4)) and experimentally (e.g. (5, 6)). Theoretical models have been developed for the case of laminar and isotropic turbulent flow. In both cases the number of collisions J_{ij} per unit volume and time between spherical particles of type i and of type j, which would occur if neither hydrodynamic nor colloidal interactions were present, can be calculated by the well-known equation derived by Von Smoluchowski (7)

$$J_{ij} = \tfrac{4}{3} * R_{ij}^3 * \gamma * N_i * N_j \qquad [1]$$

for the laminar case. In this equation R_{ij} denotes the collision radius (usually equated to $a_i + a_j$, where a_i is the radius of particle i), γ gives the shear rate, and N is the number of particles per unit volume.

If the particles are smaller than the so-called Kolmogorov length scale λ_k, the number of collisions for the case of turbulent flow is given by (8)

$$J_{ij} = 1.29 * R_{ij}^3 * \sqrt{\frac{\epsilon}{\nu}} * N_i * N_j, \qquad [2]$$

where ϵ is the energy dissipation per unit mass and time and ν is the kinematic viscosity of the dispersion medium. The Kolmogorov length scale λ_k is given by

$$\lambda_k = \left(\frac{\nu^3}{\epsilon}\right)^{0.25}. \qquad [3]$$

Hydrodynamic and colloidal forces were incorporated for equal-sized spherical particles in a uniform laminar flow field independently by Zeichner and Schowalter (1) and by van de Ven and Mason (2). The former defined a stability ratio W, giving the ratio of the number of collisions that would occur if hydrodynamic and colloidal interactions were absent (the model of Von Smoluchowski) and the actual number of collisions. The latter defined a so-called capture efficiency which is the inverse of the stability ratio. The stability ratio can be calculated by trajectory analysis. Later Adler (3) calculated capture efficiencies for the case of nonequal spherical particles.

Higashitani (4) incorporated the same model for isotropic turbulent flow in which he made use of a result by Taylor (9): for small particles the average shear rate as sensed by two particles close to each other can be given by

$$\gamma = \sqrt{\frac{2}{15\pi} * \frac{\epsilon}{\nu}}. \qquad [4]$$

The turbulent stability ratio W_T (or capture efficiency) can be calculated by the same procedure as for laminar flow.

It seems obvious to compare the coagulation behavior in different flow types, but strangely enough little effort has been made. The coagulation behaviors in some flow configurations were compared in an investigation by Ives and Al Dibouni (5). They studied the coagulation rate in laminar shear flow, in a fixed bed, and in a fluidized bed. Commercially available 1.2-μm polystyrene particles in a 0.1 M NaCl solution were used as the colloidal system. Fluidized bed

[1] To whom correspondence should be addressed.

0021-9797/95 $6.00

coagulation experiments showed significant particle aggregation; the results of coagulation in a fixed porous bed were masked by a filter effect.

Stein *et al.* (6) effected coagulation in a Couette apparatus with either a rotating inner or outer cylinder. They concluded that at a given shear rate the stability ratio in laminar shear flow is lower than in Taylor vortex flow and ascribed this phenomenon to the partial elongational character of the Taylor vortex flow.

In this study we compare the coagulation rate of monosized fully destabilized polystyrene particles in a Couette apparatus with either a rotating outer or a rotating inner cylinder, in a stirred tank, and in laminar pipe flow. We also studied the perikinetic coagulation rate. The results are compared with the theories of Zeichner and Schowalter (1), van de Ven and Mason (2), and Higashitani *et al.* (4).

Polystyrene particles were chosen as the disperse phase because very narrow particle size distributions can be obtained and because polystyrene particles have a very small density difference compared to the continuous phase we used (a NaCl solution which prevents settling). In addition, much knowledge is available about polystyrene particles in water as a colloidal system.

There are two main problems when comparing the orthokinetic coagulation efficiencies in shear fields of different character:

(a) A flow field of a given type (laminar, Taylor vortex, etc.) should be characterized with regard to its intensity, preferably by one parameter. In this respect, the volume average shear rate has been chosen, for two reasons:

(i) It can be determined for all flow types investigated here. When the flow field can be precisely described mathematically, the volume average shear rate can be calculated from equations describing the velocities; when this is not the case, as may happen, e.g., in the case of turbulent flows, the volume average shear rate can be determined experimentally from the related quantity, the energy dissipation per unit of mass of the dispersion (i.e., the power necessary to maintain the flow);

(ii) The volume average shear rate is, by reason of its connection with the power necessary for establishing the flow, of practical importance when coagulation is part of a process.

The choice of the volume average shear rate as a parameter characterizing the flow field entails that flow fields of high shear rates are overestimated with regard to the efficiencies of the collisions, since according to theory the coagulation rate is not proportional to γ but to $\gamma^{0.77}$ (1) or $\gamma^{0.82}$ (2). This will be taken into account when interpreting the data.

(b) Which parameter is to be used for comparing coagulation efficiencies? This could be done by calculating, e.g., stability ratios W or collision radii R_{ij} from experimental values, together with a value of the Hamaker constant. This, however, requires a reliable value of the Hamaker constant which is not available in the case studied here; for dispersions of polystyrene in water or aqueous solutions, literature values of the Hamaker constant differ. Therefore, we chose to calculate Hamaker constants from the experimental values of the coagulation rate. Such values of the Hamaker constants should be regarded as "apparent Hamaker constants," in order to avoid confusion with the material constant itself.

EXPERIMENTAL

Particle Preparation

Polystyrene particles were prepared by the method of Goodwin and co-workers (10–12). We used 200 ml styrene (Merck, zur Synthese, stabilized with 20 ppm 4-*tert*-butylpyrocatechol), 1.7 g $K_2S_2O_8$ (Merck, zur Analyse), and 2 g NaCl (Merck, zur Analyse). The polymerization was carried out in a 3-liter cylindrical vessel with four baffles, filled with 1500 ml twice-distilled water, at 70°C. The mixture was stirred with a six-blade stirrer at 300 rpm. After 24 h the temperature was increased to 90°C for 30 min; then the reaction was stopped by lowering the temperature. The particles were washed six times in a water/ethanol mixture (50/50) by centrifugation. Then they were dialyzed against twice-distilled water using an Amicon Model 8400 ultrafiltration cell, with 0.4-μm filters, until the conductivity of the dialysate was equal to that of the twice-distilled water (1.80 μmho). The resulting PS-latex had a number average diameter of 2.415 μm and a volume average diameter of 2.434 μm. The high degree of monodispersity assures the possibility of determining several polyplets.

Coagulation Apparatuses

We used three different apparatuses to generate different flow fields:

(i) A Couette apparatus was used in which both the outer and the inner cylinders could be rotated. The inner cylinder had a radius of 4.85 cm, the outer one had a radius of 5.00 cm, and the gap height was 3.00 cm. The cylinders were rotated by a Motomatics S586AT- motor with a KSSL-O control unit. Because the ratio of the inner radius to the gap width is large, the effect of curvature is negligible. When the outer cylinder is rotated the flow pattern is laminar and uniform throughout the gap for all rotation speeds, if the bearings are perfect and if end effects may be neglected. The shear rate is given by

$$\gamma = 4 * \omega * \frac{R_o^2 * R_i^2}{(R_o^2 - R_i^2)^2} * \ln\left(\frac{R_o}{R_i}\right). \qquad [5]$$

In this equation ω is the angular velocity, R_o is the diameter of the outer cylinder, and R_i is the diameter of the inner

cylinder. The concentric cylinder geometry with a rotating inner cylinder has been and is being studied extensively, both theoretically and experimentally. The first success in describing this type of flow was achieved by Taylor (13) who later introduced a so-called Taylor number Ta (14)

$$\mathrm{Ta} = \frac{4*R_o^2*(R_o - R_i)^4}{R_o^2 - R_i^2}*\left(\frac{\omega}{\nu}\right)^2. \qquad [6]$$

Taylor showed that there exists a critical value of this Taylor number, $\mathrm{Ta_c} = 1708$. If $\mathrm{Ta} < \mathrm{Ta_c}$, all infinitesimal axisymmetric disturbances that are periodic in the axial direction are damped and decay to zero with time. For $\mathrm{Ta} > \mathrm{Ta_c}$, some disturbances will grow with time, and a new secondary, axisymmetric flow in the form of regularly spaced horizontal toroidal vortices occurs.

Davey *et al.* (15) showed that with increasing Ta a second critical Taylor number, $\mathrm{Ta_c'}$, is reached. At $\mathrm{Ta_c'}$ the Taylor vortex flow becomes unstable and a so-called wavy vortex flow occurs. The wavy vortices have a definite frequency and move with a definite wave velocity in the azimuthal direction.

Experimentally these transitions were studied by Coles (16), who showed that the flow pattern depends on the initial conditions and on how the value of Ta is reached. Gollub and Swinney (17), Fenstermacher *et al.* (18), and Walden and Donelly (19) studied the time behavior of the flow field for increasing values of Ta beyond the critical value. They observed a transition from laminar Couette flow to steady Taylor vortex flow, a transition from Taylor vortex to periodic wavy vortex flow, a transition to quasi-periodic flow, and a transition to chaotic flow. One thing with which one has to deal is the finite annulus length effects. A good review on the subject of Couette flow has been written by DiPrima and Swinney (20).

Because theory has not kept pace with experimental work, especially at higher values of the Taylor number, we decided to measure the energy dissipation as a function of the angular velocity (see Appendix) and to calculate an average shear rate from the results.

(ii) Pipe flow was established in stainless steel pipes with lengths of 1, 2, 3, 4, 5, and 6 m and an inner diameter of 1 mm. Although the inner surface of the pipe was not perfectly smooth (it looked dull) we assumed that this did not influence the flow. This assumption was supported by the measured pressure fall, which was nearly the value as predicted by theory. The destabilized dispersion was pumped into the pipe by a large syringe whose plunger is driven by a Motomatics Motor S586AT generator, which assures a constant flow rate. The pressure fall was measured as a function of the flow rate for the different pipe-lengths and showed good agreement with the theoretically predicted ones for laminar flow. The flow will be developed completely after a pipe-length of $x = 0.056*\mathrm{Re}*2r$ (21) (with the Reynolds number $\mathrm{Re} = 2\rho vr/\eta$, where ρ is the density of the fluid, v is the mean fluid velocity, r is the radius of the pipe, and η is the viscosity). Because the highest Reynolds number in our experiments was ±2000, the maximal length after which the flow is completely developed is 0.1 m. Because the minimal pipe-length was 1 m, the effect of the flow development may be neglected. The energy-dissipation per unit of mass may be calculated from the power input P (22)

$$\epsilon = \frac{P}{V*\rho} = \frac{Q*\Delta p}{V*\rho} = \frac{8*Q^2*\eta*L}{\pi^2 R^6 L} = \frac{8Q^2\eta}{\pi^2 R^6}, \qquad [7]$$

where Q is the volume flow rate, V is the volume in which the energy is dissipated, ρ is the density of the fluid, Δp is the pressure drop across the tube, and R is the radius of the pipe. Another method for calculating the energy dissipation per unit of mass is to calculate the average shear rate from the velocity profile in the tube (22), assuming laminar flow:

$$\gamma = \frac{8Q}{3\pi R^3} \qquad [8]$$

(iii) A flat-bottomed tank equipped with four baffles and a six-blade Rushton-type impeller were chosen to generate a turbulent flow field (see Fig. 1). The tank diameter D was 0.05 m. The energy-dissipation in the tank as a function of the stirring rate can be calculated by the power number $\Phi = P/(\rho N^3 D^5)$ where P is the power input and N is the rotation speed of the stirrer, vs the Reynolds number $\mathrm{Re} = \rho N D^2/\eta$ curve as given by (23). The dissipation of energy was also measured in the same way as that used for the Couette apparatus with the inner cylinder rotating (see Appendix). The agreement between actual and theoretical values of the energy dissipation is good in view of the accuracy with which the measurements were performed. The small difference may be due to the thickness of the disc x_1, and/or the thickness of the stirrer blades (24). Another possible explanation is that all experiments described in the literature were performed on stirred tanks larger than the one used by us.

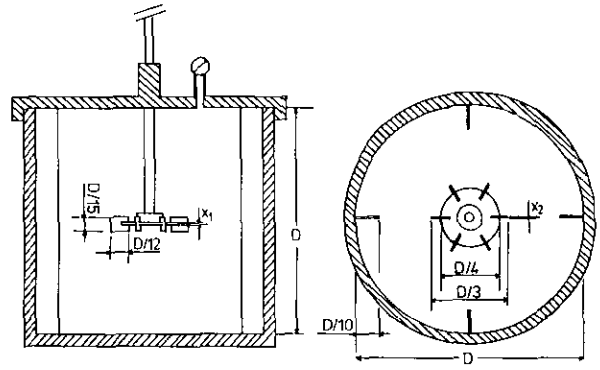

FIG. 1. The stirred tank. In our experiments $D = 0.05$ m.

Preparation of the Dispersion and Measurement Procedure

A PS dispersion with a solid volume fraction of 2×10^{-4} was prepared by suspending the required amount of particles in twice-distilled water by ultrasound (in a Branson 1200 ultrasound bath). A certain amount of this dispersion was mixed with an equal volume of a 1 *M* NaCl solution (which ensures full destabilization when the suspension is electrostatically stabilized), dispersed with ultrasound for 5 min, and poured gently into the coagulation apparatus. According to Higashitani *et al.* (25) this particle concentration is high enough to ensure rapid coagulation (rapid coagulation in turbulent flow requires not only that the electrolyte concentration be higher than the critical coagulation concentration, but also that the particle concentration surpasses the value 4.08×10^{13} m^{-3}). Because of the low solubility of polystyrene in a salt solution, occurrence of so-called polymer "hairs" is not likely to occur. It was not possible to obtain a dispersion of primary particles only: the procedure led to a dispersion of 90% primary particles. This phenomenon has been described before by other investigators (26), and is ascribed to incomplete redispersion of coagulated particles (see Figs. 2 and 3).

Samples (0.5 ml) of the dispersion were withdrawn from the coagulation unit at several times with a Finnpipette (from Labsystems OY), equipped with an oval needle. The smallest inner diameter of this needle was 1 mm, the largest was 3 mm. This needle was used because it just fitted into the gap of the Couette apparatus and thus it insured a shear rate as small as possible during the sampling.

The chosen dimensions and a sampling time of 2.5 s result in a maximal shear rate of ± 500 s^{-1}.

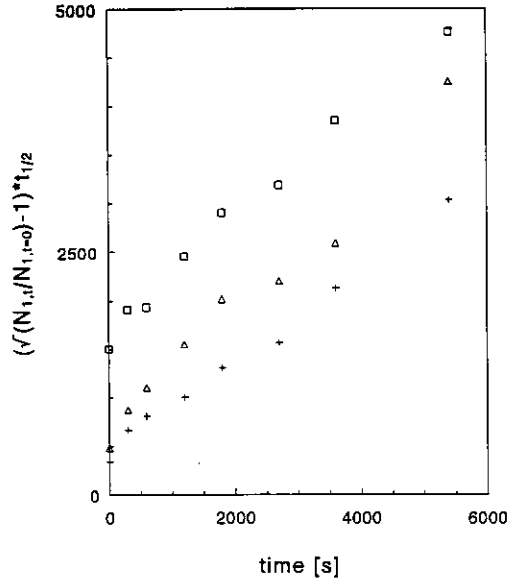

FIG. 2. Example of Brownian coagulation experiments. Different points of intersection with the vertical axis represent different initial particle size distributions.

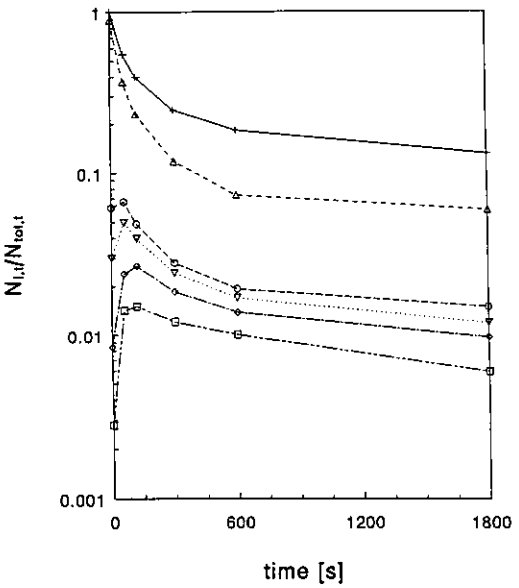

FIG. 3. The number of particles with time. Laminar flow, gamma = 200 s^{-1}. +, total number of particles; (△) singlets; (○) doublets; (▽) triplets; (◇) quartets; (□) quintets.

The samples were diluted to 25 ml with Isoton 2 (supplied by Coulter Ltd.). This dilution ensures simultaneous reduction of the particle volume fraction and of the salt concentration. It was assumed that under these conditions the coagulation rate is negligible and that the state of the dispersion is fixed.

The number of particles and their size were measured by a Coulter counter Model ZM, equipped with a Channelyzer, and a Coulter range expander. Determinations were performed with a 30-μm orifice. Aggregate breakdown in the Coulter counter results only in deviations if the different parts of the aggregate are far apart and will be seen as different particles by the apparatus. Aggregate breakdown in both the Finpippette and the Coulter counter was tested and appeared to be negligible (27). The number of particles in 50 μl were counted. Because of the narrow size distribution of the polystyrene latex, the number of several different polyplets, up to quintets, could be determined.

RESULTS AND DISCUSSION

Brownian Coagulation in the Absence of Repulsion

In the case of Brownian coagulation the measured stability can be deduced by (28)

$$\frac{N_1}{N_{1,t=0}} = \left(1 + \frac{t}{t_{1/2}}\right)^{-2}, \qquad [9]$$

in which $N_{1,t=0}$ denotes the initial number of primary particles, t is the time, and $t_{1/2}$ is a characteristic Brownian co-

agulation time in which the number of particles is reduced to half its initial value. Rewriting Eq. [9] gives:

$$t = \left(\sqrt{\frac{N_{1,t=0}}{N_1}} - 1 \right) * t_{1/2}$$

$$= \left(\sqrt{\frac{N_{1,t=0}}{N_1}} - 1 \right) * \frac{3\eta}{4kT * N_{1,t=0}} * W_{Br}. \qquad [10]$$

The stability ratio W_{Br} can thus be found by measuring the change in the number of particles, plotting $((N_{1,t=0}/N_1)^{0.5} - 1) * 3\eta/(4kTN_{1,t=0})$ as a function of the time t and calculating the slope of the curve (see Fig. 2). The slopes of the different curves show good reproducibility. Because the system consists almost entirely of single particles at the start of the experiment it is a good approximation to assume that collisions occur only between primary particles (because of small differences in the particle size distributions at $t = 0$, the abscissas in Fig. 2 are different). The condition of spherical particles introduced into the theory is met in the case of PS particles.

We performed several Brownian coagulation experiments which resulted in an average Brownian stability ratio W_{Br} of 1.76 ± 0.13. From this value and the theoretical stability ratios which can be calculated from the theory as developed by Spielman (29) one can calculate the effective Hamaker constant of the system PS in a 0.5 M NaCl solution. The average value in the case of a nonretarded attractive potential is 5.69×10^{-21} J. If we make use of the retarded potential with a London wavelength of 0.1 μm (30), the Brownian stability ratio gives an effective Hamaker constant of 7.25×10^{-20} J.

Various authors have calculated the effective Hamaker constant for the system polystyrene in water, but there is no complete agreement. Krupp *et al.* (31) give $A = 3.4 \times 10^{-21}$ J, whereas Gingell and Parsegian (32) calculated a value of $A = 9.0 \times 10^{-21}$ J at interparticle distances shorter than 10 nm, while at longer distances the value is lowered to a limiting value of $A = 3.2 \times 10^{-21}$ J.

Similar coagulation experiments have been performed by other authors (see Table 1). As can be seen from the table, the values of the stability ratios vary from 1.5 to 2.6. A problem in interpreting the data is that most of the authors do not describe the properties of their particles adequately. Many used Dow polystyrene latices as they were delivered.

Couette Apparatus; Laminar Flow

In Fig. 3 the result of an orthokinetic coagulation measurement as performed in the Couette apparatus with a rotating outer cylinder is shown. The initial coagulation rate for these experiments was determined by fitting a second-order polynome to the number of single particles vs time curve and calculating the slope for $t = 0$. Because the flow pattern is laminar and is the same throughout the apparatus the shear rate is unambiguous and the stability ratio W_{flow} can be calculated by dividing the number of collisions, as predicted by von Smoluchowski, by the actual number of collisions:

$$W_{flow} = \frac{J_s}{J} = \frac{4/3(2a)^3\gamma N_1^2}{2(dN_1/dt)_{t=0}} = \frac{4\phi\gamma}{\pi} * \left(\frac{d \ln N_1}{dt} \right)^{-1}. \qquad [11]$$

The orthokinetic stability ratio can also be calculated as a function of the dimensionless parameters $N_{SA} = 6\pi\eta a^3\gamma/A$ and $N_{RA} = 2\pi\epsilon_0\epsilon_r\psi^2 a/A$. Van de Ven and Mason (2) concluded that in the absence of repulsive forces ($N_{RA} = 0$) the stability ratio is given by

$$W_{flow} = f(\lambda_L/a) * N_{SA}^{0.18}, \qquad [12]$$

where $f(\lambda_L/a)$ is a function of the London wavelength λ_L. In the case of $a = 1$ μm and $\lambda_L = 0.1$ μm they found $f(\lambda_L/a) = 1.587$.

In Fig. 4 the values of the stability ratios are shown as a function of N_{SA}. To calculate N_{SA} we used values of $A = 3.4 \times 10^{-21}$ J, $\eta = 10^{-3}$ Pa s. Calculated values of stability ratios from Eq. [12] are also shown. The course of the calculated values agrees quite well (though not exactly) with the measurements; especially at higher N_{SA} values, the experimental stability ratio values show a tendency to be larger than those predicted from theory.

In addition, the Hamaker constant used for calculating the theoretical values represented in Fig. 4 is lower than the one best agreeing with our Brownian coagulation data. From the experimentally determined stabilities and the theoretical curve as described by Eq. [12] one can calculate the value of the effective Hamaker constant for the system of polystyrene particles in a 0.5 M NaCl solution, $A = (1.81 \pm 0.31) * 10^{-21}$ J. This value agrees reasonably with the effective Hamaker constant as determined from spectroscopic measurements by Krupp *et al.* (31): $A = 3.4 \times 10^{-21}$ J, but is

TABLE 1
Brownian Stability Ratios of Polystyrene Dispersions

Investigators	$2a$ (μm)	ϕ	[Electrolyte]	W_{Br}
Higuchi *et al.* (33)	1.83	3.21×10^{-5}	Various	1.71
Swift and Friedlander (34)	0.871	3.45×10^{-5}	2 M NaCl	2.6
Matthews and Rhodes (26)	0.714	1.91×10^{-6}	0.01 M $AlCl_3$	1.65
Matthews and Rhodes (26)	1.305	1.91×10^{-6}	0.2 M $AlCl_3$	2.1
Higashitani and Matsuni (35)	0.974	4.35×10^{-4}	1.25 M KCl	1.74
Lips *et al.* (36)	0.126	1.14×10^{-6}	0.01 M $LaNO_3$	1.5
Lichtenbelt *et al.* (37)	0.234	1.9×10^{-4}	0.05 M $BaCl_2$	2.03
Zeichner and Schowalter (38)	0.496	$1\text{-}6 \times 10^{-5}$	0.6 N NaCl	2.1
Feke (39)	0.675	2.27×10^{-5}	0.6 M NaCl	1.87

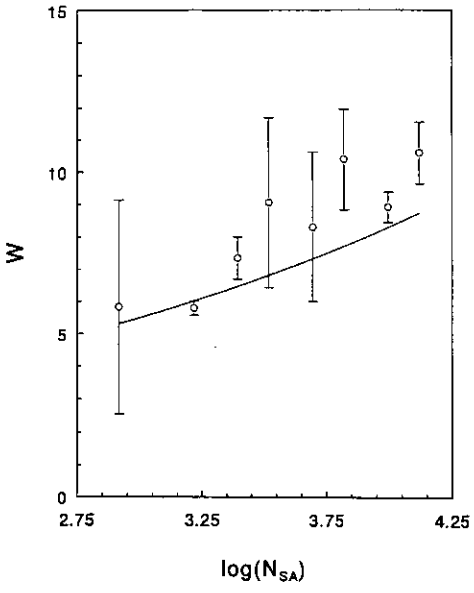

FIG. 4. Stability ratio W_{flow} as a function of $N_{SA} = 6\pi\eta a^3\gamma/A$ for the Couette with rotating outer cylinder. Bars indicate the 95% confidence interval. The line gives the theoretically predicted value of W_{flow} (1). Values for N_{SA} were calculated using a Hamaker constant A of 3.4×10^{-21} J.

lower than the value consistent with our Brownian coagulation data (7.25×10^{-20} J). In other words, orthokinetic coagulation is less effective than expected from Brownian coagulation data, even when the shear field is homogeneous to a very good degree of approximation (as in laminar flow in a narrow gap). The latter consideration excludes an explanation of the different values of the effective Hamaker constant through the use of an average shear rate based on linear averaging over the volume. The latter might be suspect as a parameter for characterizing the intensity of the flow field, because high shear rate zones contribute relatively less to the coagulation than low shear rate zones (the coagulation rate is proportional to $\gamma^{0.8}$ rather than to γ). However, this explanation is inapplicable to the case at hand because the shear field is homogeneous. The most appropriate explanation seems to be that we are dealing here with the disruption of aggregates by the shear forces exerted by the flow. Consistent with this explanation, the discrepancies between values predicted from theory, with $A = 7.25 \times 10^{-20}$ J, are greatest at high average shear rates.

Our experimental results show good agreement with the results of Curtis and Hocking (40), who performed orthokinetic coagulation on a polystyrene latex ($a = 0.998$ μm) in 0.145 M NaCl. The applied shear rate in their experiments varied from 0.633 to 112 s^{-1}. The effective Hamaker constant derived from their results was $(2.48 \pm 1.21) \times 10^{-21}$ J.

Because the Péclet number $Pe_\gamma = 3\pi\eta a^3\gamma/kT$ (where k is the Boltzman constant and T is the absolute temperature) varies from about 1300 to 21,000, the difference between the number of collisions calculated from shear only, and the number of collisions as calculated for combined Brownian and shear motion (41) is negligible.

Couette Apparatus; Taylor Vortex Flow

Above a certain critical Taylor number, so-called Taylor vortices will occur. By flow visualization, the onset of Taylor vortex flow at about the expected angular velocity ($\omega = 2.55$ s^{-1}) was observed; at higher angular velocities more turbulences were seen, but the characteristic pattern of this type of flow could be recognized even at the largest ω values employed.

In Fig. 5 the coagulation rate J_{11} is shown as a function of the energy dissipation per unit mass of the suspension ϵ (the method of measuring the energy dissipation per unit mass and time is described in the Appendix). Also shown are the results of the laminar Couette experiments.

For the case of $\omega = 2.62$ s^{-1} corresponding with $\epsilon^{0.5} = 0.086$ m^2 s^{-3} or $N_{SA} = 2.91$, the flow of the Couette with a rotating inner cylinder is still laminar ($Ta < Ta_c$) and at this rotation rate the shear is the same for the rotating inner and outer cylinders. The stability ratio for this angular velocity can thus be calculated and shows good agreement with the one determined from the experiment in the Couette apparatus with a rotating outer cylinder. However, at higher ω values, in the Couette apparatus with a rotating inner cylinder the shear rate cannot be determined unambiguously. If Taylor vortices are present, the shear rate as calculated by Eq. [5] (assuming laminar flow) is too low. Van Atta (42) stated that at the onset of the Taylor instability the annulus is not filled with fluid in turbulent motion, but the axial secondary

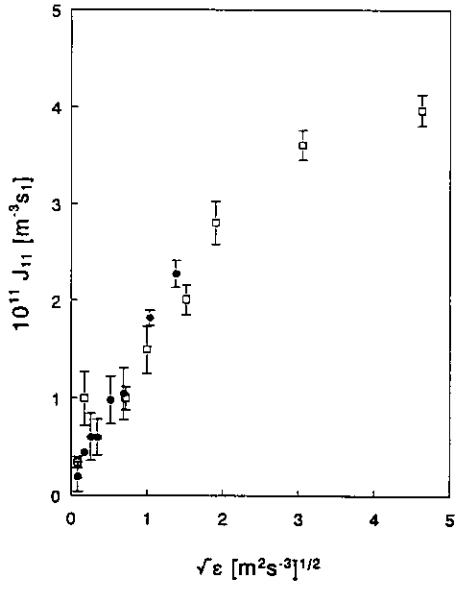

FIG. 5. Collision rate J_{11} as a function of the energy dissipation for the Couette apparatus with a rotating inner cylinder. Bars indicate the 95% confidence interval. □, inner cylinder rotating; ●, outer cylinder rotating.

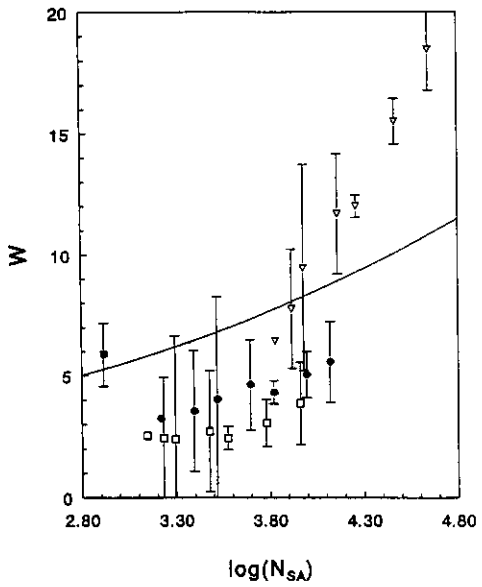

FIG. 6. The stability ratio W_{flow} as a function of $N_{SA} = 6\pi\eta a^3\gamma/A$ for γ calculated in different ways: (●) $\gamma = \gamma$ (Eq. [5]); (▽) $\gamma = (\epsilon/\nu)^{0.5}$ (Eq. [13]); (□) $\gamma = (2/(15\pi))^{0.5}*(\epsilon/\nu)^{0.5}$ (Eq. [4]); Values for N_{SA} were calculated using a Hamaker constant A of 3.4×10^{-21} J.

flow is confined to spiral bands embedded in a nearly laminar tangential flow.

Koh *et al.* (43) proposed a way to calculate an effective shear rate γ_{eff} on the basis of equal energy input

$$\gamma_{eff} = \sqrt{\gamma_{lam}^2 + \gamma_{vor}^2} \qquad [13]$$

with γ_{lam} given by Eq. [5] and $\gamma_{vor} = (\epsilon/\nu)^{0.5}$. The value of γ_{vor} can be obtained by subtracting the laminar dissipation rate from the total dissipation rate. The effective shear rate thus calculated can also be given by $\gamma_{eff} = (\epsilon_{tot}/\nu)^{0.5}$, where ϵ_{tot} is the total energy dissipation per mass unit.

Using the values for the average shear rates calculated from this equation and the experimentally determined values for the energy dissipation, results in a W_{flow} vs N_{SA} plot as given by Fig. 6. A theoretical curve, calculated on the basis of a shear rate given by Eq. [13], using $A = 3.4 \times 10^{-21}$ J, is shown in the figure as well. It seems that the functional dependence of W_{flow} on N_{SA} is different from the theoretical one. Though a definitive explanation is at present not available, the following possibilities are considered: (a) it is difficult to describe Taylor vortex flow correctly; (b) the high stability ratios at high values of N_{SA} indicate disruption of aggregates being important in this region; and (c) because of the heterogeneity of the flow field, the average shear rate found by linear averaging over the volume is not a suitable parameter.

The shear rate could also be calculated by assuming laminar flow (Eq. [5]) or isotropic turbulent flow (Eq. [4]).

TABLE 2
Calculated Effective Hamaker Constants for Taylor Vortex Flow

γ (s^{-1})	A (J)
γ (Eq. [5])	$(6.03 \pm 1.98) \times 10^{-20}$
$(\epsilon/\nu)^{0.5}$ (Eq. [13])	$(2.21 \pm 1.90) \times 10^{-21}$
$(2/15\pi)^{0.5}*(\epsilon/\nu)^{0.5}$ (Eq. [4])	$(6.35 \pm 4.01) \times 10^{-19}$

The resulting effective Hamaker constant in these cases then is given in Table 2.

From these results the approximation for the shear rate as given by $(\epsilon/\nu)^{0.5}$ seems to be best, because the calculated values of the stability ratio fit best to the theoretical ones. The fact that the values of the stability ratio for the higher values of N_{SA} are too high may be caused by underestimation of the shear rate. It may also be that aggregate disruption plays a role at these energy dissipation rates.

Pipe Flow

As can be seen in Fig. 7 the coagulation rate in pipe flow is about the same as in the case of the Couette flow regimes. Making use of Eq. [8] we can calculate the stability ratio W_{flow}. The results are also shown in Fig. 7. As can be seen the experimental values for W_{flow} agree very well with the theoretically predicted ones. Calculating a effective Hamaker constant from the stability ratios gives $A = (3.68 \pm 1.67) \times 10^{-21}$ J.

Stirred Tank

In Fig. 8 the coagulation rate J_{11} is shown as a function of the energy dissipation per unit of mass ϵ. Also shown are

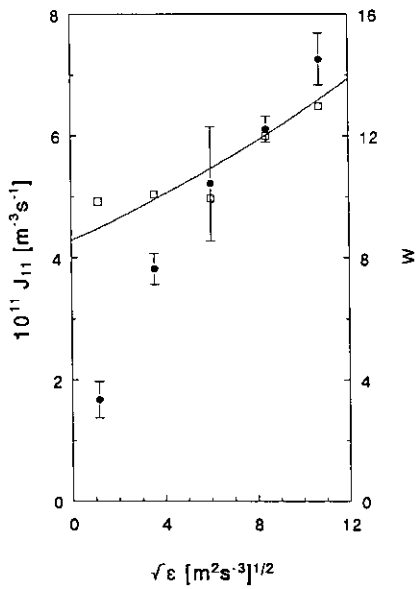

FIG. 7. Collision rate J_{11} (●) and stability ratio W_{flow} (□) as a function of the energy-dissipation for pipe flow. (—) theoretically predicted stability ratio.

the experimental results of Higashitani *et al.* (25), who used a 2.17-μm polyvinyltoluene latex in a 0.75 M KCL solution. They performed their coagulation experiments in a tank equipped with four baffles and used an eight-blade stirrer. The coagulation rates of their experiments have been calculated from their experimental stability vs N_{SA} plot (their Fig. 10). The agreement between our results and the results of Higashitani *et al.* is very good.

The line in Fig. 8 is the theoretical curve as calculated from the model of Higashitani *et al.* [4]. The turbulent stability ratio W_T was calculated from an effective Hamaker constant of 3.4×10^{-21} J and making use of Eq. [4] to calculate an average sensed shear rate. Although the model predicts coagulation rates which are somewhat too high, the agreement is good, especially at the lower energy dissipations. This is rather astonishing in view of the simplicity of the model employed (particles stay within the same eddy and no collisions occur between particles in different eddies; the hydrodynamic interaction is taken to be the same as in laminar flow).

Koh *et al.* (43) developed a compartmentalized model for batch flocculation in which they used an effective mean shear rate equal to the volume average value obtained from the first moment of the shear rate distribution. Comparison of turbulent coagulation rates with laminar ones shows that the latter ones are higher at equal energy dissipation. This is in accordance with theory; at equal energy dissipation the number of collisions is the same for both laminar and isotropic turbulent flow if hydrodynamic interactions are neglected ($W_{flow} = W_T = 1$):

$$J_{11,turbulent} = 1.29(2a)^3 \sqrt{\frac{\epsilon}{\nu}} * N_1^2 \qquad [14]$$

$$J_{11,laminar} = \tfrac{4}{3} * (2a)^3 * \gamma * N_1 = \tfrac{4}{3} * (2a)^3 * \sqrt{\frac{\epsilon}{\nu}} * N_1^2. \qquad [15]$$

But because the shear rate which is sensed by the colliding particles is lower for the isotropic turbulent flow $\gamma = (2/(15\pi))^{0.5} * (\epsilon/\nu)^{0.5}$ than for the laminar case $\gamma = (\epsilon/\nu)^{0.5}$, the stability ratio W_T is smaller than the ratio W_{flow} and thus the coagulation rate is higher for the isotropic turbulent flow.

CONCLUSION

The perikinetic coagulation rate of a polystyrene latex with a diameter of 2.4 μm in a 0.5 M NaCl solution is higher than predicted by the model of Spielman (29) (the Brownian stability ratio W_{Br} is lower). This is, however, in good agreement with measurements performed by other researchers.

The coagulation rate in laminar Couette flow can be predicted by the model of Van de Ven and Mason or Zeichner and Schowalter, but the effective Hamaker constant best describing the data (0.34×10^{-20} J) is lower than that describing perikinetic coagulation (7.25×10^{-20} J). This entails that orthokinetic coagulation in laminar flow is slower than expected from isotropic turbulent flow (as predicted by the model of Higashitani)

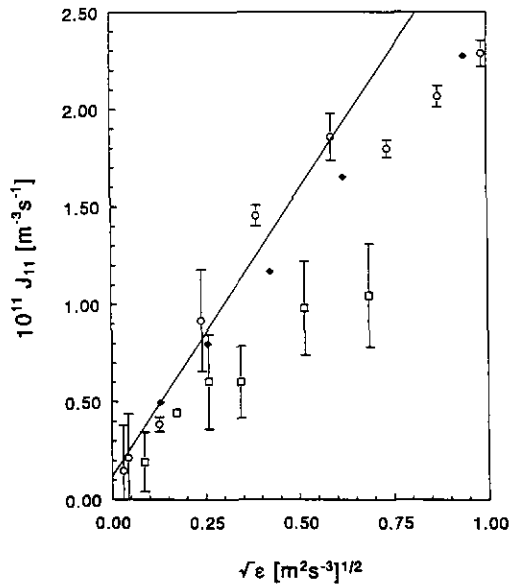

FIG. 8. Collision rate J_{11} as a function of the energy dissipation for the stirred tank geometry. (□) Couette laminar flow; (○) stirred tank; (♦) experiments by Higashitani; (—) model by Higashitani.

—at equal energy dissipation the shear rate as sensed by two particles approaching each other is higher for the laminar flow case ($\gamma = (\epsilon/\nu)^{0.5}$ than for the turbulent flow case ($\gamma = (2/15\pi)^{0.5}(\epsilon/\nu)^{0.5}$);

—as a consequence of the lower sensed shear rate in turbulent flow the stability ratio for this case is lower than for the laminar flow;

—because at equal energy dissipation the number of collisions is the same for both laminar and isotropic turbulent flow, but the stability ratio is lower in the latter case, the coagulation rate is higher in turbulent flow, which is found experimentally.

APPENDIX: MEASUREMENT OF THE ENERGY DISSIPATION

In the case of a Couette apparatus the energy dissipation can be calculated if the torque T on the outer cylinder is known

$$\epsilon = \frac{T\omega}{V\rho} = \frac{F_i R_i \omega}{V\rho} = \frac{F_o R_o \omega}{V\rho}, \qquad [A1]$$

where ω is the angular velocity, V is the volume in which the energy is dissipated, ρ is the density of the dispersion, F_i

and F_o are the force on the inner and on the outer cylinder, respectively, and R_i and R_o are the radius of the inner and of the outer cylinder.

The problem in measuring the torque on the outer cylinder is that the bearings are not without friction. Therefore we measured the minimum force F_{M1} required to let the outer cylinder rotate in the same direction as the inner one

$$F_{M1} = F_W - F_H, \qquad [A2]$$

in which F_W is the force due to the friction of the bearings and F_H is the hydrodynamic force of the fluid acting on the outer cylinder.

The minimum force required to let the outer cylinder rotate in the opposite direction as the inner cylinder is

$$F_{M2} = F_W + F_H. \qquad [A3]$$

From Eq. [A2] and [A3] the force F_o can be calculated ($F_o = F_H = (F_{M2} - F_{M1})/2$) and thus the energy dissipation can be determined.

The experimental setup was as follows. A small lightweight vial was connected to the outer cylinder of the Couette apparatus by means of a wire. The rotation rate of the inner Couette cylinder was set to the desired value and water was added to the vial until the outer Couette cylinder started to rotate. The experiment was repeated with the inner cylinder rotating at the same rate in the opposite direction. From the two water masses in the vial, F_{M1} and F_{M2}, can be calculated and thus F_H and F_0, at different rotation rates of the inner cylinder.

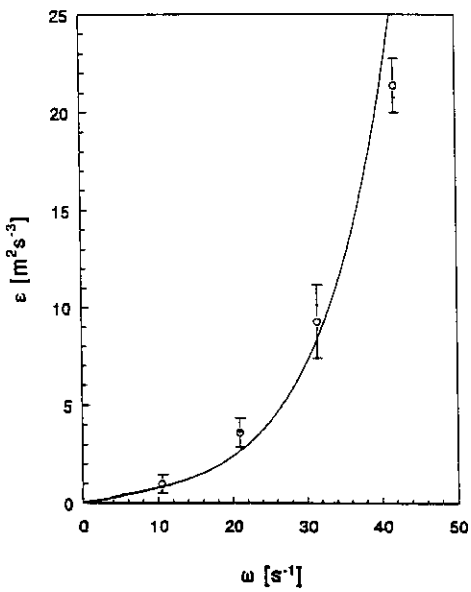

FIG. A1. The measured energy dissipation in the Couette apparatus with a rotating inner cylinder as a function of the angular velocity. The curve is the fitted model of Donelly.

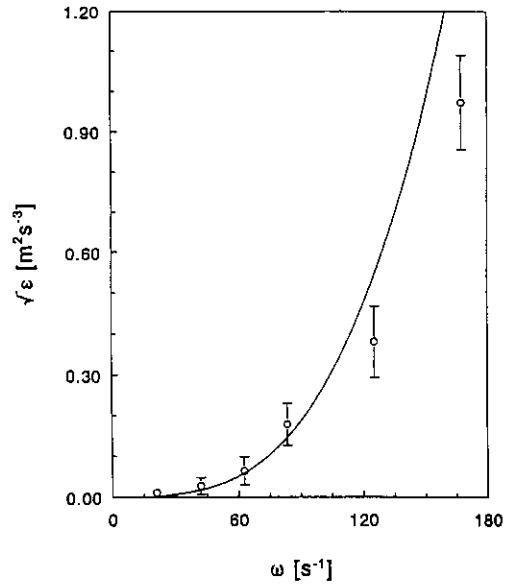

FIG. A2. The measured energy dissipation in the stirred tank as a function of the angular velocity. (O) measured values; (—) values predicted from Holland's power curve.

The results for the Couette apparatus with a rotating inner cylinder is given in Fig. A1. According to Donelly (44), the torque for high angular velocities can be written as

$$T = a*\omega^{1.5}. \qquad [A4]$$

Fitting our results to this equation gives $a = 2.551 \times 10^{-5}$. This curve also is shown in Fig. A1.

The same experiments were performed for the stirred tank. The results are shown in Fig. A2, together with the values as predicted from the power curve by Holland *et al.* (23). The agreement between the two curves is good. The differences between the two curves at high angular velocities might be due to the thickness of the stirrer blades, a parameter which is not in the model of Holland.

REFERENCES

1. Zeichner, G. R., and Schowalter, W. R., *AIChE J.* **23,** 243 (1977).
2. Van de Ven, T. G. M., and Mason, S. G., *Colloid Polym. Sci.* **255,** 794 (1977).
3. Adler, P. M., *J. Colloid Interface Sci.* **83,** 461 (1981).
4. Higashitani, K., Ogawa, R., Hoshawa, G., and Matsumo, Y., *J. Chem. Eng. Jpn.* **15,** 299 (1982).
5. Ives, K. J., Al Dibouni, M., *Chem. Eng. Sci.* **34,** 983 (1979).
6. Stein, H. N., Logtenberg, E. H. P., van Diemen, A. J. G., and Peters, P. J., *Colloids Surf.* **18,** 223 (1986).
7. Von Smoluchowski, *Z. Phys. Chem.* **92,** 155 (1917).
8. Saffman, P. G., and Turner, J. S., *J. Fluid Mech.* **10,** 16 (1956).
9. Taylor, G. I., *Proc. R. Soc. London A* **151,** 421 (1935).
10. Goodwin, J. W., Hearn, J., Ho, C. C., and Ottewill, R. H., *Br. Polym. J.* **5,** 347 (1973).
11. Chung-li, Y., Goodwin, J. W., and Ottewill, R. H., *Prog. Colloid Polym. Sci.* **60,** 163 (1976).

12. Goodwin, J. W., Ottewill, R. H., Pelton, R., Vianello, G., and Yates, D. E., *Br. Polym. J.* **10,** 173 (1978).
13. Taylor, G. I., *Philos. Trans. R. Soc. London Ser. A* **223,** 289 (1923).
14. Taylor, G. I., *Proc. R. Soc. London A* **157,** 546 (1936).
15. Davey, A., Diprima, R. C., and Stuart, J. T., *J. Fluid Mech.* **31,** 17 (1968).
16. Coles, D., *J. Fluid Mech.* **21,** 385 (1965).
17. Gollub, J. P., and Swinney, H. L., *Phys. Rev. Lett.* **35,** 927 (1975).
18. Fenstermacher, P. R., Swinney, H. L., and Gollub, J. P., *J. Fluid Mech.* **94,** 103 (1979).
19. Walden, R. W., and Donelly, R. J., *Phys. Rev. Lett.* **42,** 301 (1979).
20. Diprima, R. C., and Swinney, H. L., *in* "Hydrodynamic Instabilities and the Transition to Turbulence" (H. L. Swinney and J. P. Gollub, Eds.), p. 139. Springer, New York, 1981.
21. Friedman, M., Gillis, J., and Liron, N., *Appl. Sci. Res.* **19,** 426 (1968).
22. Gregory, J., *Chem. Eng. Sci.* **36,** 1789 (1981).
23. Holland, F. A., and Chapman, F. S., "Liquid Mixing and Processing in Stirred Vessels," Reinhold, Chapman & Hall, London, 1966.
24. Bujalski, W., Nienow, A. W., Chatwin, S., and Cooke, M., *Chem. Eng. Sci.* **42,** 317 (1987).
25. Higashitani, K., Yamanchi, K., Matsuno, Y., and Hosakawa, G., *J. Chem. Eng. Jpn.* **16,** 299 (1983).
26. Matthews, B. A., and Rhodes, C. T., *J. Pharm. Sci.* **57,** 557 (1968).
27. Krutzer, L. L. M., "The Influence of Flow Type, Particle Type and Gravity on Orthokinetic Coagulation," PhD. Thesis, Eindhoven University of Technology, Eindhoven, 1993.
28. Kruyt, H. R., "Colloid Science, Volume 1, Irreversible Systems." Elsevier, Amsterdam, 1952.
29. Spielman, L. A., *J. Colloid Interface Sci.* **33,** 562 (1970).
30. Gregory, J., *Adv. Colloid Interface Sci.* **17,** 149 (1982).
31. Krupp, H., Schnabel, W., and Walter, G., *J. Colloid Interface Sci.* **39,** 423 (1972).
32. Gingell, D., and Parsegian, V. A., *J. Colloid Interface Sci.* **44,** 456 (1973).
33. Higuchi, W. I., Okada, R., Stelter, G. A., and Lemberger, A. P., *J. Pharm. Sci.* **52,** 49 (1963).
34. Swift, D. L., and Friedlander, S. K., *J. Colloid Sci.* **19,** 621 (1964).
35. Higashitani, K., and Matsuno, Y., *J. Chem. Eng. Jpn.* **12,** 460 (1979).
36. Lips, A., Smart, C., and Willis, E., *Trans. Faraday Soc.* **67,** 2979 (1973).
37. Lichtenbelt, J. W. Th., Pathmamanoharan, C., and Wiersema, P. H., *J. Colloid Interface Sci.* **49,** 281 (1974).
38. Zeichner, G. R., and Schowalter, W. R., *J. Colloid Interface Sci.* **71,** 148 (1979).
39. Feke, D. L., "Kinetics of Flow-Induced Coagulation with Weak Brownian Diffusion," Ph.D. Thesis, Princeton University, Princeton, NJ, 1981.
40. Curtis, A. S. G., and Hocking, L. M., *Trans. Faraday Soc.* **66,** 1381 (1970).
41. Feke, D. L., and Schowalter, W. R., *J. Fluid Mech.* **133,** 17 (1985).
42. Van Atta, C., *J. Colloid Interface Sci.* **50,** 307 (1975).
43. Koh, P. T. L., Andrews, J. R. G., and Uhlherr, P. H. T., *Chem. Eng. Sci.* **39,** 975 (1984).
44. Donelly, R. J., and Simon, N. J., *J. Fluid Mech.* **7,** 401 (1960).